NMR IN BIOMEDICINE
NMR Biomed. 2006;**19**:69–76
Published online 12 January 2006 in Wiley InterScience (www.interscience.wiley.com). DOI:10.1002/nbm.1002

The role of vessel maturation and vessel functionality in spontaneous fluctuations of T_2*-weighted GRE signal within tumors

Christine Baudelet,[1] Greg O. Cron,[1] Réginald Ansiaux,[1] Nathalie Crokart,[1] Julie DeWever,[2] Olivier Feron[2] and Bernard Gallez[1]*

[1]Laboratory of Biomedical Magnetic Resonance and Laboratory of Medicinal Chemistry and Radiopharmacy, Université Catholique de Louvain, Avenue E. Mounier 73.40, B-1200 Brussels, Belgium
[2]Unit of Pharmacology and Therapeutics, Université Catholique de Louvain, Avenue E. Mounier 73.40, B-1200 Brussels, Belgium

Received 15 December 2004; Revised 18 July 2005; Accepted 19 September 2005

ABSTRACT: Acute hypoxia (transient cycles of hypoxia-reoxygenation) is known to occur in solid tumors and is generally believed to be caused by tumor blood flow instabilities. It was recently demonstrated that T_2*-weighted (T_2*w) gradient echo (GRE) MRI is a powerful non-invasive method for investigating periodic changes in tumor pO_2 and blood flow associated with acute hypoxia. Here, the possible correlation between tumor vessel immaturity, vessel functionality and T_2*w GRE signal fluctuations was investigated. Intramuscularly implanted FSa II fibrosarcoma-bearing mice were imaged at 4.7 T. Maps of spontaneous fluctuations of MR signal intensity in tumor tissue during air breathing were obtained using a T_2*w GRE sequence. This same sequence was also employed during air–5% CO_2 breathing (hypercapnia) and carbogen breathing (hypercapnic hyperoxia) to obtain parametric maps representing vessel maturation and vessel function, respectively. Vascular density, vessel maturation and vessel perfusion were also assessed histologically by using CD31 labeling, α-smooth muscle actin immunoreactivity and Hoechst 33242 labeling, respectively. About 50% of the tumor fluctuations occurred in functional tumor regions (responsive to carbogen) and 80% occurred in tumor regions with immature vessels (lack of response to hypercapnia). The proportion of hypercapnia-responsive voxels were found to be twice as great in fluctuating than in non-fluctuating tumor areas (P: 0.22 vs 0.13). Similarly, the proportion of functional voxels was somewhat greater in fluctuating tumor areas (P: 0.54 vs 0.43). The mean values of MR signal changes during hypercapnia (VD) and during carbogen breathing (VF) (significant voxels only) were also larger in fluctuating than in non-fluctuating tumor areas ($P < 0.05$). This study demonstrated that adequate vessel functionality and advanced vessel maturation could explain at least in part the occurrence of spontaneous T_2*w GRE signal fluctuations. Functionality and maturation are not required for signal fluctuations, however, because a large fraction of fluctuations could still occur in non-perfused and/or immature vessels. Copyright © 2006 John Wiley & Sons, Ltd.

KEYWORDS: tumor; acute hypoxia; blood flow; fluctuations; BOLD; blood oxygen level-dependent MRI; carbogen; vessel maturation

INTRODUCTION

Acute hypoxia (i.e. transient cycles of hypoxia–reoxygenation) is known to occur in solid tumors (1) and may be a poorly-appreciated therapeutic problem as it can be associated with resistance to radiation therapy (2–6), impaired delivery of chemotherapeutic agents (7) or metastasis development (8). Although the origin of acute hypoxia is not firmly established, it is generally believed that it results from tumor blood flow instabilities. Acute hypoxia occurs in tumor cells nourished by blood vessels subject to partial and/or intermittent decreases in functionality, thereby reducing oxygen and nutrient delivery (9–11). Several factors may contribute to flow fluctuations, including arteriolar vasomotion (12,13) and rapid vascular modeling (14). Other contributory factors are functional abnormalities resulting from disorganized vascular hierarchy. Such abnormalities include non-uniform axial distribution of red blood cells within the vessel, disproportionate cell partitioning at bifurcations, non-linear flow properties of blood and other hemodynamic effects (15). Increased transcapillary permeability

**Correspondence to:* B. Gallez, Laboratory of Biomedical Magnetic Resonance, and Laboratory of Medicinal Chemistry and Radiopharmacy, Université Catholique de Louvain, Avenue E. Mounier 73.40, B-1200 Brussels, Belgium.
E-mail: Gallez@cmfa.ucl.ac.be
Contract/grant sponsor: Belgian National Fund for Scientific Research; *Contract/grant number:* 7.4503.02.
Contract/grant sponsor: Fonds Joseph Maisin.
Contract/grant sponsor: 'Actions de Recherches Concertées'—Communauté Française de Belgique; *Contract/grant number:* ARC 04/09-317.

Abbreviations used: BOLD, blood oxygen level-dependent; GRE, gradient echo; SI, signal intensity; SPFI, spontaneous fluctuation index; T_2*w, T_2*-weighted; VD, MR signal changes during hypercapnia; VF, MR signal changes during carbogen breathing; VFI, vascular functional index; VMI, vascular maturation index; α-SMA, α-smooth muscle actin.

Copyright © 2006 John Wiley & Sons, Ltd.

is another functional abnormality of tumor vasculature that could be responsible for instability of blood flow. Mollica *et al*. demonstrated that in the presence of moderate leakiness, the fluid dynamics of tumor circulation evolve toward a sustained oscillatory response, in both the microvascular pressure and blood flow (16). All these functional abnormalities characterizing tumor vessels are linked to structural abnormalities. In tumors, wall structure and branching patterns of vessels are highly abnormal (17). The mural cells, pericytes and vascular smooth muscle cells are either absent or loosely associated with the tumor endothelium (18). Vessel immaturity could therefore be an important factor leading to temporal heterogeneities of blood flow and oxygenation in tumors.

T_2*-weighted (T_2*w) gradient echo (GRE) MRI can be used to provide *in vivo* imaging of tumor vessel maturation and functionality (19–21). This technique is sensitive to changes in deoxyhemoglobin content manifested as change in T_2*, referred to as the blood oxygen level-dependent (BOLD) effect. Thereby a change in T_2*w GRE signal intensity can result from changes in tumor blood hemoglobin oxygen saturation, hematocrit, blood volume or blood flow (red blood cells flux). GRE sequences are also sensitive to changes in plasma flow via changes in the apparent T_1 relaxation (22,23). Maturation of the tumor vasculature can be determined from changes in T_2*w GRE images in response to hypercapnia (elevation of inhaled CO_2) (19–21). Vascular reactivity to hypercapnia occurs in mature vessels covered with smooth muscle cells which respond to elevated levels of arterial CO_2. This method has been used to predict the vascular response to anti-angiogenic and anti-vascular treatments (21,24). On the other hand, functional status of the tumor vascular bed can be assessed from T_2*-w GRE images during a carbogen (95% O_2, 5% CO_2) breathing challenge. High-oxygen gas breathing produces acute changes in blood oxygenation in the functional tumor vascular bed, resulting in the BOLD contrast effect.

T_2* weighed MRI also holds promise for studying the transient hypoxia phenomenon. Thus, it was recently demonstrated that T_2*w GRE MRI could be used to provide both temporal and detailed spatial information on spontaneous fluctuations of blood flow and/or oxygenation in tumor vasculature throughout the tumor (25).

In the present study, the possible correlation between tumor vessel immaturity, vessel functionality and spontaneous T_2*w GRE MRI signal fluctuations were investigated, the latter being related to the pathophysiology of acute hypoxia in tumors (25).

MATERIALS AND METHODS

Animal protocols

Syngeneic FSa II fibrosarcomas were inoculated into the hind leg muscle of male C3H/HeOuJIco mice ($n = 10$). MRI measurements were performed when tumors were 8 ± 1 mm in diameter (8–9 days later). Mice were anaesthetized using 1.2% isoflurane in air administered with a face mask. Anesthetized mice were placed prone and were immobilized using adhesive tape. Warm air was flushed into the magnet to maintain the body temperature at 37 °C.

MRI

MRI was performed with a 4.7 T (200 MHz, ^{1}H) 40 cm inner diameter bore system (Bruker Biospec, Ettlingen, Germany). A surface coil, 2 cm in diameter, was used for radiofrequency transmission and reception. T_2w anatomical images were acquired using a fast spin-echo sequence [repetition time (TR) = 3 s, effective echo time (TE) = 63 ms]. A single 1.3 mm thick slice was localized such that it passed through the tumor center. For T_2*-w GRE imaging the following parameters were used: $TR = 200$ ms, $TE = 18$ ms, flip angle = 45 °, 12.5 kHz receiver bandwidth, 64 phase and frequency encode steps, linear encoding order, 3 cm field of view, two averages, 25.6 s/image. Two runs of 140 sequential images (one run per hour) were acquired. For the first run, mapping of spontaneous fluctuations was performed during air breathing. For the second run, maturation and functionality of the tumor vasculature were determined from the GRE images acquired during inhalation of air (first 30 scans), air containing 5% CO_2 (next 20 scans), air again (20 scans), carbogen (95% O_2, 5% CO_2, 30 scans), then again air (final 20 scans).

Data analysis

MRI data were analyzed using in-house programs written in the Interactive Data Language (RSI, Boulder, CO, USA). A region of interest (ROI) encompassing the tumor was drawn manually on the T_2w anatomical image. Each voxel in this region of interest was subsequently analyzed for both GRE runs. Tumor size was estimated by calculating the surface from the ROI, which represents the largest tumor section.

Fluctuating zones maps. Viewing the series of images in cine mode ensured the absence of disturbing motion. A power spectrum analysis was performed to identify which temporal signals were significantly different from Gaussian-distributed white noise (25). The significance level α was set to 0.025. Analysis of the first run during air breathing yielded a spontaneous fluctuation map of the tumor area. The spontaneous fluctuation index (SPFI), namely the fraction of tumor area that displayed T_2*w GRE signal intensity (SI) fluctuations during the one hour of air breathing, was computed.

Copyright © 2006 John Wiley & Sons, Ltd.

Vessel functionality and vessel maturation maps. By means of statistical parametric mapping, we generated vascular functional and vascular maturation maps from the second data run. Image regression analysis was performed using the general linear model approach (26). The hemodynamic response under gas mixture breathing was found to be best modeled by a ramped boxcar (gradual linear increase or decrease for four scans at each end of the boxcar), instead of using a simple rectangular boxcar function. A set of discrete cosine functions ($n = 2$) was also included in the design matrix to model low-frequency confounds. Appropriate contrast weights were used to test the null hypothesis of no change in SI during inhalation of CO_2 or carbogen, which corresponds to zero amplitude of the boxcar waveform (the significance level α was set to 0.01). The absolute values of the changes in SI due to hypercapnia and carbogen breathing (VD and VF, respectively) were recorded for each voxel. VD was only estimated when VF was found to be significant (i.e. functional vasculature). The fraction of mature vessels among total functioning vessels (vascular maturation index or VMI) and the percentage of functional tumor area (vascular functional index or VFI) were also calculated. Linear regression analysis was performed to assess the correlation between the different indices. A *t*-test was used for the significance of the correlation coefficient.

Histology

Histological data were obtained from another cohort of mice ($n = 7$) to correlate with the fluctuating zones maps.

Administration of fluorescent dye H33342. Immediately following MRI (1 h of imaging under air breathing), mice received an intravenous injection of the DNA-binding fluorescent Hoechst 33342 dye (Aldrich Chemicals, Gillingham, Dorset, UK), (0.5% w/v in saline, 20 mg/kg), for subsequent analysis of the perfusion status of tumor vessels. The time interval between the injection of Hoechst 33342 dye and killing of the mice was 1 min.

Immunostaining. Tumors were removed and frozen. Care was taken to section the tumor in the same plane as MRI. Hence mice were kept in the same position as during MRI and, before tumor resection, the top and center of the tumor were marked with ink lines. Frozen sections of tumor of 5 µm thickness were cut. Sections were counterstained with Mayer's hematoxylin to allow correct slice identification and selection. Staining for the vascular endothelial cell-specific marker CD31 was performed with a rat monoclonal antibody against CD31 (PharMingen), revealed with a secondary antibody coupled to a Tetramethyl Rhodamine IsothioCyanate fluorophore (TRITC). Detection of smooth muscle tumor was achieved by α-smooth muscle actin (α-SMA) staining using purified mouse monoclonal anti-α-SMA conjugated with fluorescein isothiocyanate (FITC) isomer I (Sigma-Aldrich, Bornem, Belgium). Cryoslices were then examined with a Zeiss, Axioskop microscope (Zavantem, Belgium) equipped for fluorescence. Images were stored as digital files and viewed with Photoshop 7.0 (Adobe, Mountain View, CA, USA). Whole tumor images were reconstituted by merging individual images.

RESULTS

Figure 1 shows an example of a spontaneous MR signal fluctuations pattern of a tumor voxel and its hemodynamic response during hypercapnia and carbogen breathing.

Zones of spontaneous T_2*w MR signal fluctuations occupied $21 \pm 3\%$ (mean $\pm$ SE) of the tumor area. In a previous study fluctuating voxels were classified into two classes: (i) true fluctuations (i.e. sequential signal increase and decrease) and (ii) signal drop with no recovery (25). Little or no signal drop was observed among voxels in the tumors used in the present study. However, when this occurred, voxels with signal drop were excluded using a cluster analysis (27).

Carbogen-responsive areas represented $50 \pm 5\%$ (mean $\pm$ SE) of the total tumor area, whereas $17 \pm 3\%$ (mean $\pm$ SE) only of the tumor was responsive to hypercapnia. The proportion of voxels with significant VD was found to be significantly greater in fluctuating than in non-fluctuating area: 22% of all fluctuating voxels have a significant VD and 13% of all non-fluctuating voxels (Table 1, A.). From these calculations, it could be observed also that the majority (78%) of fluctuating areas were located in tumor regions with absence of response to

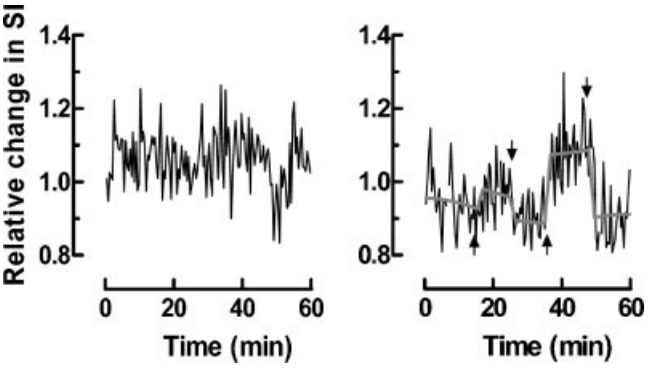

Figure 1. Left: time course of T_2*w MR signal of a tumor voxel showing spontaneous fluctuations during air breathing (sudden signal increase at $t = 2$ min and signal drop at $t = 50$ min with subsequent recovery). Right: corresponding time course of signal change for air–5% CO_2 gas mixture breathing (15–25 min) and carbogen breathing (35–50 min). The fit of the estimated general linear model is displayed over these data. Arrows indicate the start/stop of hypercapnia and carbogen breathing

Copyright © 2006 John Wiley & Sons, Ltd.

Table 1. Distribution of mature (A) and functional (B) voxels according to the presence of MR signal fluctuations and distribution of fluctuating voxels according to vessel maturity and functionality (C): comparison of proportions

Proportions	Yes	No	P^a
(A) Mature voxels			
MR fluctuations	0.22	0.13	<0.001
(B) Functional voxels			
MR fluctuations	0.54	0.43	<0.001
(C) Fluctuating voxels			
Maturity (hypercapnia responsiveness)	0.28	0.18	<0.001
Functionality (carbogen responsiveness)	0.22	0.16	<0.001

[a]Z-test for comparing two observed proportions.

hypercapnia. The proportion of voxels with significant VF was found significantly greater in fluctuating than in non-fluctuating areas and 54% of fluctuating areas are located in carbogen-responsive regions (Table 1, B.); see also Fig. 2. Tumor areas with hypercapnia responsiveness had a higher probability of fluctuations than non-responsive regions (Table 1, C.). The same trend is observed when analyzing the carbogen responsiveness (Table 1, C.).

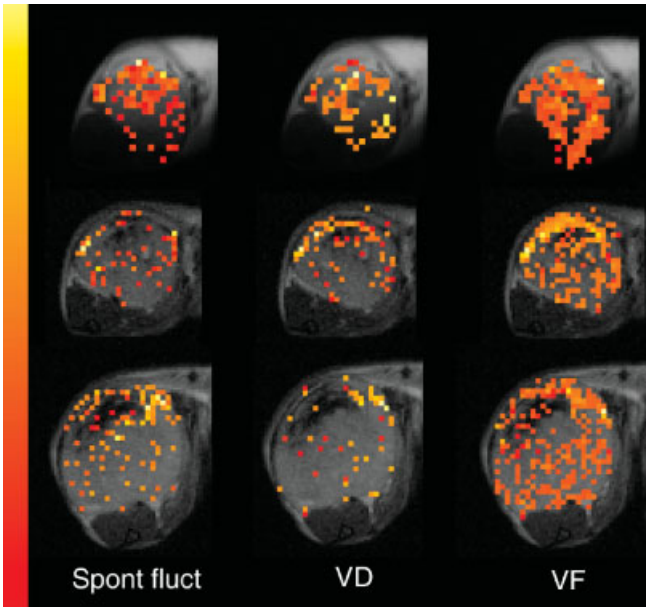

Figure 2. Co-registration of spontaneous fluctuations, vascular maturation and vascular function maps for three separate intramuscular FSa II fibrosarcoma tumors in mice. Left: spontaneous fluctuations maps determined by spectral analysis of T_2*w GRE imaging during the 1 h of air breathing. Middle: vascular maturation (VD) maps. Right: vascular function (VF) maps. The last two types of maps represent significant GRE MRI signal changes during air–5%CO_2 breathing and carbogen breathing, respectively. The color scale is a function of the variance of the time series (for the spontaneous fluctuations maps) (25) or the extent of signal change (for the VD and VF maps). Parameters are in arbitrary units: from red (minimum) to yellow (maximum). Note that the proportion of mature and functional vessels are greater in tumor areas demonstrating spontaneous T_2*w GRE SI fluctuations than in non-fluctuating areas

Histological results showed that FSa-II tumors were well vascularized as indicated by numerous CD31 (endothelial marker) positive spots uniformly distributed among the tumor [Fig. 3(B)]. The number of α-SMA-immunoreactive cells (presumably to be found on arterioles, venules and capillaries) in tumors was small and less abundant than inside the muscle tissue. Occasionally, arterioles were found inside the tumor tissue, covered by circumferentially arranged α-SMA-immunoreactive smooth muscle cells [Fig. 3(E)]. Examination of Hoechst 33342 labeling showed heterogeneity of distribution of functional vasculature [Fig. 3(D)]. Fluctuating areas were located mostly in perfused tumor areas (central part of tumor in Fig. 3). In these perfused areas, there was not a high incidence of α-SMA immunoreactivity [Fig. 3 (A)–(C)]. The few regions with positively-staining α-SMA immunoreactivity (situated primarily in the periphery for this particular tumor), however, presented a high incidence of signal fluctuations. Therefore, although most of the signal fluctuations occurred in regions with immature vessels, the presence of mature vessels did not preclude the occurrence of signal fluctuations.

Continuing with MR results, it was observed that the averages of the significant values for VD and VF were greater for fluctuating voxels than for non-fluctuating voxels ($P<0.05$ for both, paired t-tests) (Fig. 4). In addition, VF values were greater than VD values ($P<0.01$, paired t-test), indicating greater signal changes upon carbogen breathing than upon air–CO_2 breathing. Furthermore, there was a significant correlation between SPFI and VFI ($r=+0.66$) and a weak positive correlation between SPFI and VMI ($r=+0.53$) (Table 2). There was no significant correlation between SPFI and tumor size ($r=-0.14$) and a small inverse correlation between VFI and tumor size ($r=-0.50$) (Table 2). There was also a strong correlation between whole tumor-averaged VF and the vascular functional index, VFI ($r=+0.92$, $P<0.001$, t-test) (Fig. 5).

The vascular functional index VFI was $50\pm5\%$ (mean $\pm$ SE) and the vascular maturation index VMI was $34\pm3\%$ (mean $\pm$ SE).

DISCUSSION

In this study, it was investigated whether tumor vessel immaturity and functionality, as measured by the effect of hypercapnia and carbogen breathing on MR signal changes, could explain the occurrence of the spontaneous T_2*w MR signal fluctuations in tumors. The results indicate that more than 50% of the spontaneous T_2*w MR signal fluctuations were observed in regions with functional vasculature (as detected by actual responsiveness to carbogen breathing), suggesting a vascular origin

Copyright © 2006 John Wiley & Sons, Ltd.

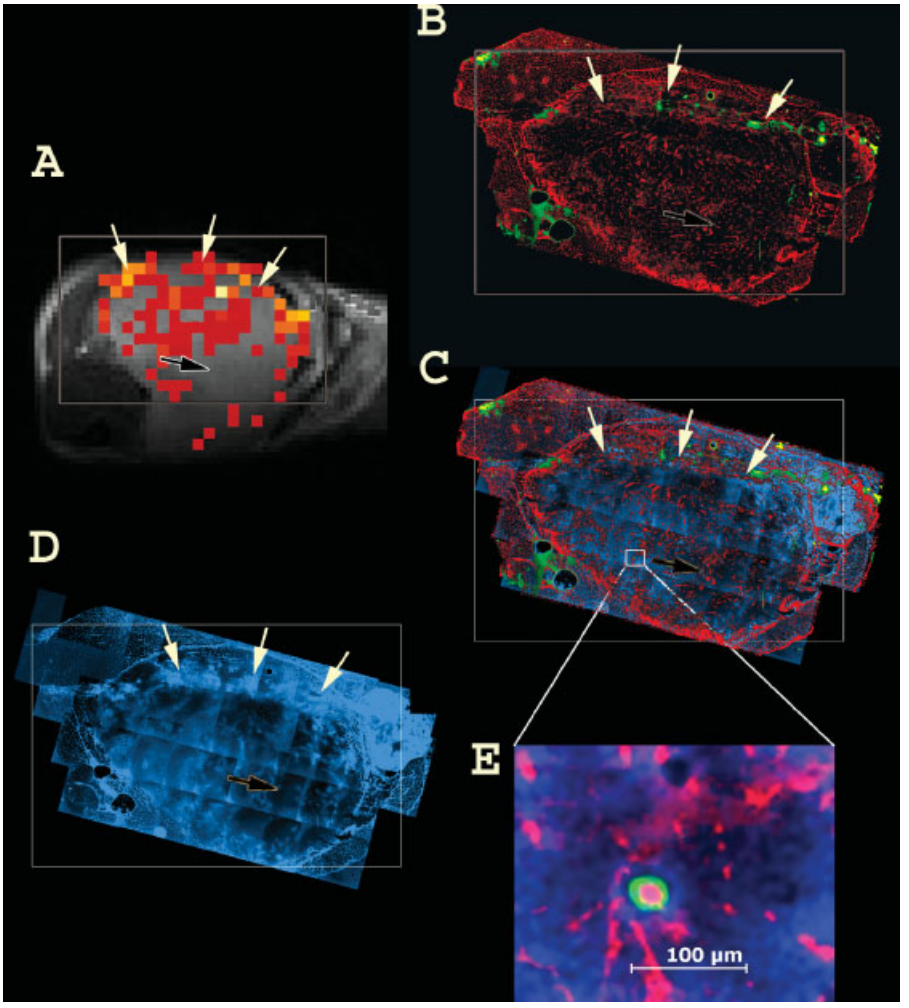

Figure 3. Comparison of MRI with histology. (A) Map of spontaneous T_2*w GRE SI fluctuations in a FSa II tumor. (B) Double staining for CD31-immunoreactive endothelial cell (red) and α-SMA-immunoreactivity (mature vessels) (green). (C) Triple staining for CD31 (red),α-SMA (green) and Hoechst 33342 (blue). (D) Hoechst 33342 labeling assay (perfusion marker). (E) Inset. Enlargement of a tumor area showing an arteriole surrounded with α-SMA-positive cells (green). MR signal fluctuations were found typically in the tumor rim [white arrows in (A)] and also in a more centrally located tumor area. Those areas could be related mostly to perfused tumor areas [see (D)]. A large portion of the tumor did not experience signal fluctuations [black arrow in (A)]. This tumor region was typically located in a non-perfused area as indicated by absence of Hoechst 33342 labeling [see (D)]. Poor α-SMA-immunoreactivity was observed [see (B) and (C), green] but when present was located in fluctuating areas

for these fluctuations. This can be related to previous results, which showed that the true fluctuations (i.e. sequential signal increase and decrease) in FSa tumors were found preferentially (70%) in regions accessible to an MR Gd-based contrast agent, i.e. regions for which vessels are not clamped (25). In line with this, it was also found in the present study that the proportion of voxels with significant change upon carbogen breathing was greater in tumor regions that fluctuate than in those that do not fluctuate. In addition, there was a significant positive correlation between SPFI and VFI, indicating that the better the tumor is perfused, the greater is the incidence of spontaneous fluctuations. It should be noted that no significant correlation with the tumor size was observed. Histological findings correlated with the MR results. Indeed, it was observed that the fluctuating tumor areas were associated mostly to perfused vessels (as indicated by Hoechst 33342 labeling and CD31 immunoreactivity).

The results also suggest that there is still a large proportion of the MR signal fluctuations (46%) which occur in non-functional regions. This implies that either some vascular responses to carbogen escaped detection or that, in fact, there actually were no responses to carbogen in these tumor areas at the time of the measurement. If the former scenario is correct, the vascular response is likely

Copyright © 2006 John Wiley & Sons, Ltd.

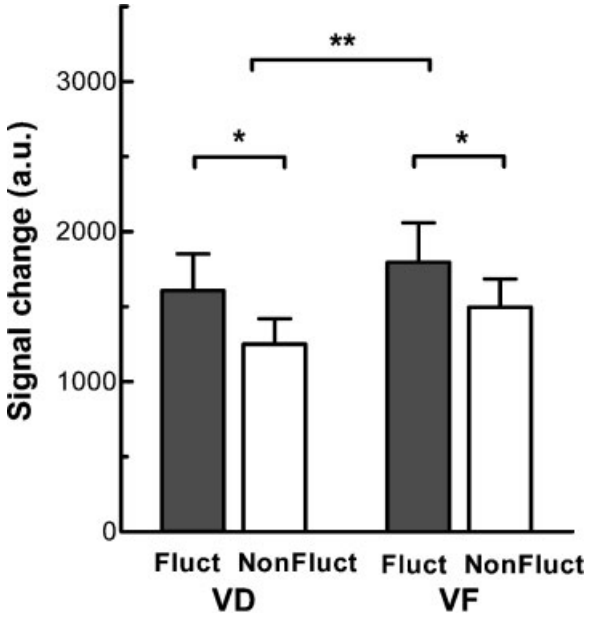

Figure 4. Mean of statistically significant absolute signal changes during hypercapnia (VD) and during carbogen breathing (VF). The values are greater for fluctuating than for non-fluctuating tumor areas. VF values are also larger than the VD values. $*P < 0.05$, $**P < 0.01$; paired *t*-test. Values are means ± SE, $n = 10$

too small in certain voxels to be detected [poor signal-to-noise ratio in regions with low blood volume and small vessel size (28)]. Lowering the statistical threshold for testing the significance of signal changes would yield a higher percentage of functional tumor area (VFI) but would also increase beta-type errors (false positives). In fact, several reasons support the latter scenario (i.e. no vascular response to carbogen at the time of measurement). First, dramatic changes in vascular functionality, including complete stoppage of blood flow, might occur just after the observed fluctuations (i.e. just after the first run of GRE imaging). Although the incidence of this phenomenon is low (5%), sudden total vascular stasis has been observed to occur in tumors using matched dye methods or intravital microscopy (3,13). Events such as vascular collapse, vessel plugging by leukocytes or impingement of tumor cells on the vascular lumen could lead to vascular stasis. Second, it could be that certain vessels are already so well oxygenated that changes in deoxygenated hemoglobin content upon carbogen breathing would be too small to provide significant BOLD contrast. Third, T_2*w GRE fluctuations could also be related to tumor vessel growth (14) and thus such fluctuations could also occur in non-functional tumor areas. Patan *et al*. described rapid vascular remodeling associated with microvascular growth (14). Vascular sprouting and pillar formation occurred at a frequency of up to three per hour. Finally, it could be that part of the MR signal fluctuations observed in the present study are not caused by dynamic changes in T_2* due to changes in the oxyHb/deoxyHb ratio, but rather by plasma flux variations. Indeed, the T_2*w GRE sequence is sensitive to changes in both deoxyhemoglobin content (T_2* contrast) and also plasma blood flow (inflow effect, T_1 contrast) (22). In tumors, an uneven distribution of red cell fluxes in microvessels can lead to plasma channels (i.e. vessels carrying no red blood cells) (1). In plasma channels, it is not clear if carbogen would produce a signal change (via an inflow effect), but it is clear that in the absence of red cells, there is no chance of modification of deoxyhemoglobin content.

Table 2. Linear coefficient correlations between spontaneous fluctuations index (SPFI), vascular functional index (VFI), vascular maturation index (VMI) and tumor size: estimated values and statistical significance (*P*)

r	SPFI	*P*	VFI	*P*	VMI	*P*
VFI	+0.66	0.03	1			
VMI	+0.53	0.11	+0.35	0.33	1	
Tumor size	−0.14	0.70	−0.50	0.14	−0.24	0.050

[a]Correlations relate to individual animals, $N = 10$, *t*-test.

Only a small part (22%) of the functional tumor area experienced MR signal fluctuations, suggesting that vessel functionality does not guarantee the presence of fluctuations. This proportion might have been larger if a longer imaging time had been employed. Indeed, increasing the imaging time window could help to reveal voxels exhibiting fluctuations over longer periods of time (25). For example, using the hypoxia marker mismatch technique, it has been observed that the number of transiently hypoxic tumor cells increases with the duration of marker exposure (29). Also, using a fiber-optic oxygen-sensing device it has been demonstrated that different regions within the same tumor may show acute hypoxia with different kinetics (30). Although longer imaging times could provide a more confident mapping of parts of the tumor with temporal heterogeneity of blood flow and/or

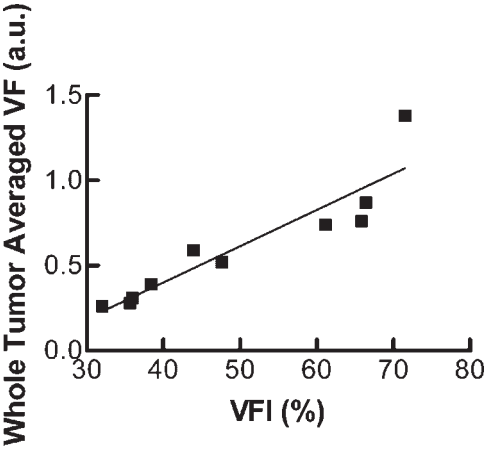

Figure 5. Correlation between the percentage of functional tumor area (VFI) and the whole tumor averaged change in SI during carbogen breathing (VF). Each point represents one individual mouse

Copyright © 2006 John Wiley & Sons, Ltd.

oxygen levels, adverse effects of the resulting longer anesthesia time would have to be taken into account.

Concerning the degree of vessel maturation with regard to the occurrence of MR fluctuations, it was observed that the majority of fluctuating areas were located in immature tumor regions, as revealed by lack of signal change during hypercapnia and absence of α-SMA immunoreactivity. This supports the concept that absence of pericytes/vascular smooth vessel cells, a sign of structural abnormality of tumor vessels, can contribute to functional abnormalities such as blood flow fluctuations (18). In addition, the proportion of mature vessels was even greater in tumor regions that fluctuate, suggesting that vasomotion of mature vessels may still play a role, although minor in this tumor line, in generating fluctuant hypoxia. These findings corroborate the work of Intaglietta *et al*. (12) and Dewhirst *et al*. (13), who demonstrated the link between vasomotion and red cell flux variation by monitoring spontaneous changes in tumor arteriolar diameter.

By analyzing the magnitude of the hemodynamic response upon carbogen breathing (VF), it was observed that VF was greater for fluctuating than for non-fluctuating tumor areas. VF can be viewed as a marker of the density of functional microvessels in tumor (high VF values, high density) (20,28). It is not entirely surprising that T_2*w GRE fluctuations were more likely associated with regions with particularly high vascular densities. Indeed, the high BOLD contrast sensitivity of regions with a highly perfused vascular volume could make the acute change in red cell flux and/or blood oxygenation more easily detectable (28).

Also, there was an excellent correlation between whole tumor-averaged magnitude of response to carbogen (VF) and the percentage of functional tumor area (VFI). This indicates that VF is itself a good general indication of how well a tumor is perfused. The advantage of VF over VFI is that it is easy to calculate and does not require voxel-by-voxel analysis (whole tumor-averaged signal is sufficient).

Finally, it should be kept in mind that extrapolation of the present results obtained on murine fibrosarcomas to other tumors requires additional investigations, given the importance of physiology (e.g. vessel maturity) between different tumor lines (e.g. murine vs xenografts).

CONCLUSION

This study demonstrated that in this tumor model, adequate vessel functionality and advanced vessel maturation could explain at least in part the occurrence of spontaneous T_2*w GRE signal fluctuations. Functionality and maturation are not required, however, since a large fraction of fluctuations can still occur in non-perfused and/or immature vessels.

Acknowledgements

This research was supported by the Belgian National Fund for Scientific Research (Grant 7.4503.02), the Fonds Joseph Maisin and the 'Actions de Recherches Concertées'—Communauté Française de Belgique (ARC 04/09-317).

REFERENCES

1. Dewhirst MW. Concepts of oxygen transport at the microcirculatory level. *Semin. Radiat. Oncol.* 1998; **8**: 143–150.
2. Cardenas-Navia LI, Yu D, Braun RD, Brizel DM, Secomb TW, Dewhirst MW. Tumor-dependent kinetics of partial pressure of oxygen fluctuations during air and oxygen breathing. *Cancer Res.* 2004; **64**: 6010–6017.
3. Chaplin DJ, Olive PL, Durand RE. Intermittent blood flow in a murine tumor: radiobiological effects. *Cancer Res.* 1987; **47**: 597–601.
4. Denekamp J, Dasu A. Inducible repair and the two forms of tumour hypoxia – time for a paradigm shift. *Acta Oncol.* 1999; **38**: 903–918.
5. Kirkpatrick JP, Cardenas-Navia LI, Dewhirst MW. Predicting the effect of temporal variations in PO_2 on tumor radiosensitivity. *Int. J. Radiat. Oncol. Biol. Phys.* 2004; **59**: 822–833.
6. Rofstad EK, Maseide K. Radiobiological and immunohistochemical assessment of hypoxia in human melanoma xenografts: acute and chronic hypoxia in individual tumours. *Int. J. Radiat. Biol.* 1999; **75**: 1377–1393.
7. Durand RE. Intermittent blood flow in solid tumours – an underappreciated source of 'drug resistance'. *Cancer Metastasis Rev.* 2001; **20**: 57–61.
8. Cairns RA, Kalliomaki T, Hill RP. Acute (cyclic) hypoxia enhances spontaneous metastasis of KHT murine tumors. *Cancer Res.* 2001; **61**: 8903–8908.
9. Braun RD, Lanzen JL, Dewhirst MW. Fourier analysis of fluctuations of oxygen tension and blood flow in R3230Ac tumors and muscle in rats. *Am. J. Physiol* 1999; **277**: H551–H568.
10. Chaplin DJ, Hill SA. Temporal heterogeneity in microregional erythrocyte flux in experimental solid tumours. *Br. J. Cancer* 1995; **71**: 1210–1213.
11. Kimura H, Braun RD, Ong ET, Hsu R, Secomb TW, Papahadjopoulos D, Hong K, Dewhirst MW. Fluctuations in red cell flux in tumor microvessels can lead to transient hypoxia and reoxygenation in tumor parenchyma. *Cancer Res.* 1996; **56**: 5522–5528.
12. Intaglietta M, Myers RR, Gross JF, Reinhold HS. Dynamics of microvascular flow in implanted mouse mammary tumours. *Bibl. Anat.* 1977; **15**: 273–276.
13. Dewhirst MW, Kimura H, Rehmus SW, Braun RD, Papahadjopoulos D, Hong K, Secomb TW. Microvascular studies on the origins of perfusion-limited hypoxia. *Br. J. Cancer Suppl.* 1996; **27**: S247–S251.
14. Patan S, Munn LL, Jain RK. Intussusceptive microvascular growth in a human colon adenocarcinoma xenograft: a novel mechanism of tumor angiogenesis. *Microvasc. Res.* 1996; **51**: 260–272.
15. Kiani MF, Pries AR, Hsu LL, Sarelius IH, Cokelet GR. Fluctuations in microvascular blood flow parameters caused by hemodynamic mechanisms. *Am. J. Physiol* 1994; **266**: H1822–H1828.
16. Mollica F, Jain RK, Netti PA. A model for temporal heterogeneities of tumor blood flow. *Microvasc. Res.* 2003; **65**: 56–60.
17. Jain RK. Molecular regulation of vessel maturation. *Nat. Med.* 2003; **9**: 685–693.
18. Morikawa S, Baluk P, Kaidoh T, Haskell A, Jain RK, McDonald DM. Abnormalities in pericytes on blood vessels and endothelial sprouts in tumors. *Am. J. Pathol.* 2002; **160**: 985–1000.
19. Neeman M, Dafni H, Bukhari O, Braun RD, Dewhirst MW. In vivo BOLD contrast MRI mapping of subcutaneous vascular function and maturation: validation by intravital microscopy. *Magn. Reson. Med.* 2001; **45**: 887–898.

Copyright © 2006 John Wiley & Sons, Ltd.

20. Gilead A, Meir G, Neeman M. The role of angiogenesis, vascular maturation, regression and stroma infiltration in dormancy and growth of implanted MLS ovarian carcinoma spheroids. *Int. J. Cancer* 2004; **108**: 524–531.
21. Abramovitch R, Dafni H, Smouha E, Benjamin LE, Neeman M. In vivo prediction of vascular susceptibility to vascular susceptibility endothelial growth factor withdrawal: magnetic resonance imaging of C6 rat glioma in nude mice. *Cancer Res.* 1999; **59**: 5012–5016.
22. Howe FA, Robinson SP, McIntyre DJ, Stubbs M, Griffiths JR. Issues in flow and oxygenation dependent contrast (FLOOD) imaging of tumours. *NMR Biomed.* 2001; **14**: 497–506.
23. Baudelet C, Gallez B. How does blood oxygen level-dependent (BOLD) contrast correlate with oxygen partial pressure (pO2) inside tumors? *Magn Reson Med* 2002; **48**: 980–986.
24. Gross DJ, Reibstein I, Weiss L, Slavin S, Stein I, Neeman M, Abramovitch R, Benjamin LE. The antiangiogenic agent linomide inhibits the growth rate of von Hippel–Lindau paraganglioma xenografts to mice. *Clin. Cancer Res.* 1999; **5**: 3669–3675.
25. Baudelet C, Ansiaux R, Jordan BF, Havaux X, Macq B, Gallez B. Physiological noise in murine solid tumours using T_2*-weighted gradient-echo imaging: a marker of tumour acute hypoxia? *Phys. Med. Biol.* 2004; **49**: 3389–3411.
26. Friston KJ, Holmes AP, Poline JB, Grasby PJ, Williams SC, Frackowiak RS, Turner R. Analysis of fMRI time-series revisited. *Neuroimage* 1995; **2**: 45–53.
27. Baudelet C, Gallez B. Cluster analysis of BOLD fMRI time series in tumors to study the heterogeneity of hemodynamic response to treatment. *Magn. Reson. Med.* 2003; **49**: 985–990.
28. Robinson SP, Rijken PF, Howe FA, McSheehy PM, van der Sanden BP, Heerschap A, Stubbs M, van der Kogel AJ, Griffiths JR. Tumor vascular architecture and function evaluated by non-invasive susceptibility MRI methods and immunohistochemistry. *J. Magn. Reson. Imaging* 2003; **17**: 445–454.
29. Bennewith KL, Durand RE. Quantifying transient hypoxia in human tumor xenografts by flow cytometry. *Cancer Res.* 2004; **64**: 6183–6189.
30. Brurberg KG, Graff BA, Rofstad EK. Temporal heterogeneity in oxygen tension in human melanoma xenografts. *Br. J. Cancer* 2003; **89**: 350–356.

Copyright © 2006 John Wiley & Sons, Ltd.